energies

MDPI

Article

Enhancing Thermal Conductivity of SiC Matrix Pellets for Accident-Tolerant Fuel via Atomic Layer Deposition of Al_2O_3 Coating

Yumeng Zhao [1,2], Wenqing Wang [3], Jiquan Wang [1,2,*], Xiao Liu [3], Yu Li [1,2], Zongshu Li [1,2], Rong Chen [3,*] and Wei Liu [2]

[1] CNNC Key Laboratory on Fabrication Technology of Reactor Irradiation Special Fuel Assembly, Baotou 014035, China
[2] China North Nuclear Fuel Co., Ltd., Baotou 014035, China
[3] School of Mechanical Science and Engineering, Huazhong University of Science and Technology, Wuhan 430074, China
* Correspondence: 17602240957@163.com (J.W.); rongchen@mail.hust.edu.cn (R.C.)

Abstract: This study investigates the enhancement of thermal conductivity in silicon carbide (SiC) matrix pellets for accident-tolerant fuels via atomic layer deposition (ALD) of alumina (Al_2O_3) coatings. Pressure-holding ALD protocols ensured precursor saturation, enabling precise coating control (0.09 nm/cycle). The ALD-coated Al_2O_3 layers on SiC particles were found to be more uniform while minimizing surface oxidation compared to traditional mechanical mixing. Combined with yttria (Y_2O_3) additives and spark plasma sintering (SPS), ALD-coated samples achieved satisfactory densification and thermal performance. Results demonstrated that 5~7 wt.% ALD-Al_2O_3 + Y_2O_3 achieved corrected thermal conductivity enhancements of 14~18% at 100 °C., even with reduced sintering aid content, while maintaining sintered densities above 92% T.D. (theoretical density). This work highlights ALD's potential in fabricating high-performance, accident-tolerant SiC-based fuels for safer and more efficient nuclear reactors, with implications for future optimization of sintering processes and additive formulations.

Keywords: SiC-based coated particle dispersed fuel; atomic layer deposition; Al_2O_3 sintering aid; accident tolerant fuel

check for updates

Academic Editor: Dan Gabriel Cacuci

Received: 5 March 2025
Revised: 12 April 2025
Accepted: 16 April 2025
Published: 21 April 2025

Citation: Zhao, Y.; Wang, W.; Wang, J.; Liu, X.; Li, Y.; Li, Z.; Chen, R.; Liu, W. Enhancing Thermal Conductivity of SiC Matrix Pellets for Accident-Tolerant Fuel via Atomic Layer Deposition of Al_2O_3 Coating. *Energies* **2025**, *18*, 2130. https://doi.org/10.3390/en18082130

Copyright: © 2025 by the authors. Licensee MDPI, Basel, Switzerland. This article is an open access article distributed under the terms and conditions of the Creative Commons Attribution (CC BY) license (https://creativecommons.org/licenses/by/4.0/).

1. Introduction

Since the Fukushima Daiichi accident in 2011, significant international attention has been directed toward the development of accident-tolerant fuels (ATFs) that offer enhanced accident tolerance and inherent safety [1–3]. Among these, ceramic-based coated particle dispersed fuels (CDFs), which incorporate TRistructural-ISOtropic (TRISO) fuel particles within a ceramic matrix, have emerged as promising candidates for advanced light water reactors (LWRs). This is attributed to their exceptional containment of fission products, outstanding corrosion resistance of the matrix, and high thermal conductivity [4–7].

The TRISO particles were initially developed in Germany, and the concept of TRISO particles dispersed in a silicon carbide (SiC) matrix was proposed by Oak Ridge National Laboratory (ORNL, USA) [8]. The SiC matrix, characterized by its high thermal conductivity and superior in-service performance, can significantly reduce the center temperature of the fuel pellets and protect the embedded TRISO particles from mechanical loading and corrosive damage [9,10]. As a strong covalent-bonded high-temperature ceramic, however,

SiC has an extremely low self-diffusion rate, which limits mass transport during the sintering process [11]. Therefore, achieving high densification through diffusion-controlled solid-state sintering alone is challenging.

Current sintering techniques primarily involve the addition of sintering aids to enhance the solid-state diffusion rate of SiC [12–15] or to generate a liquid–glass phase that facilitates the viscous flow of SiC particles [11], thereby improving the density. Commonly used sintering aids are alumina (Al_2O_3) and yttria (Y_2O_3). Al_2O_3 and Y_2O_3 can form three types of low-melting-point eutectic compounds depending on their ratios: $Y_3Al_5O_{12}$ (yttrium aluminum garnet, YAG, melting point 1760 °C), $YAlO_3$ (yttrium aluminum perovskite, YAP, melting point 1850 °C), and $Y_4Al_2O_9$ (yttrium aluminum monoclinic, YAM, melting point 1940 °C). By increasing the content of Al_2O_3 in the sintering aids and maintaining sufficient dwell time at 1400 °C, YAG can be formed prematurely, which promotes the rapid densification of the sintered samples [10].

Atomic layer deposition (ALD) is a cutting-edge thin-film fabrication technique renowned for its atomic-level precision, conformality, and uniformity. Based on sequential, self-limiting surface reactions, ALD enables the deposition of ultrathin films with sub-nanometer thickness control, making it indispensable for applications requiring high-quality coatings on complex geometries or high-aspect-ratio structures [16–18].

The development of ATFs demands advanced fabrication techniques to optimize thermal conductivity in ceramic matrices. Among core–shell production methods, ALD stands out for its ability to deposit uniform coatings, which reduce interfacial defects critical for heat transfer in SiC-based fuels. Interfacial defects (e.g., pores and oxide layers) increase phonon scattering, thereby degrading thermal conductivity. Compared to alternative methods, chemical vapor deposition (CVD) enables conformal coatings, but its limited thickness control (>10 nm) and higher process temperatures (>500 °C) risk SiC oxidation and phase degradation, compromising thermal performance [15,17,19]. Though cost-effective and scalable, sol–gel-derived coatings suffer from non-uniformity due to solvent evaporation and cracking during drying, often necessitating higher sintering aid content to compensate for defects [18]. Solution combustion synthesis (SCS) achieves moderate elemental uniformity but typically requires excess sintering additives to stabilize the core–shell structure, which degrades thermal conductivity [20]. Precipitation or impregnation methods, while offering better compositional control than mechanical mixing, face challenges in achieving nanoscale uniformity across high-surface-area powders [21]. Mechanical mixing acts as a baseline in this study, which might introduce inhomogeneous additive distribution and localized oxidation, limiting densification and heat transfer efficiency [10].

If ALD technology is combined with the addition of sintering aids, that is, by depositing sintering aids on SiC powders using ALD, it is expected to achieve a more uniform mixture of SiC and sintering aids compared to traditional mechanical mixing processes. This offers a new possibility to enhance the sintering performance of the SiC matrix or reduce the amount of sintering aids required while maintaining consistent sintering performance.

ALD of Al_2O_3 on SiC substrates has garnered significant attention for advancing high-performance electronic and optoelectronic devices [22,23]. The self-limiting nature of ALD ensures conformal coverage on SiC's complex surfaces, addressing challenges posed by its crystallographic anisotropy. However, few studies have been applied in the nuclear fuel field. SiC powders used for nuclear fuel also have special requirements, such as high purity, β-phase, and nanoscale powders, which pose new challenges to the ALD process.

This study investigates the potential of using ALD technology to deposit Al_2O_3 sintering aid on SiC powders to enhance the sintering performance of the SiC matrix. The ALD process for depositing Al_2O_3 on SiC powders was optimized, and the microstructures of the raw SiC powders and powders obtained through different mixing processes were

characterized in detail. Spark plasma sintering (SPS) was employed to densify the various mixed powders, and the density and thermal conductivity of the sintered SiC matrix samples were evaluated. The findings of this research can provide new directions for optimizing the performance of SiC-based accident-tolerant fuels.

2. Materials and Methods

2.1. Raw Materials

The selection of raw materials referred to previous studies [10]. Two types of high-purity microscale 3C-SiC (β-SiC) matrix powders (purities >99.8%, Huzhou Yuanqin New Materials Co., Ltd., Huzhou, China) were used. The β-SiC powders were mainly different in granularity, and the mass ratio of the large-particle powder (denoted as L-SiC) to the small-particle powder (denoted as S-SiC) was 1:1 to ensure the uniform particle size distribution of the mixed powder. The Al_2O_3 and Y_2O_3 powders were employed as sintering aids with purities >99.5% and granularities of 60~70 nm, and the powders were provided by Huzhou Yuanqin New Materials Co., Ltd. The morphologies of sintering aids were observed before, where the Al_2O_3 powder particles exhibited a flocculent structure with significant agglomeration, and the Y_2O_3 powder particles showed better sphericity [10].

2.2. Preparation of SiC Pellets

The mixing methods of SiC and sintering aids included mechanical mixing, ALD, and a combination of ALD and mechanical mixing. In the mechanical mixing method, the SiC powder and sintering aids (the mass ratio of Al_2O_3 to Y_2O_3 was 1:1) were mixed via wet ball milling in the agate mill jar for 4~48 h. The wet ball milling medium was anhydrous ethanol with a powder, with a grinding media ratio of 1:4. The amount of anhydrous ethanol added was 50~150 mL per 100 g of mixed powder. After ball milling, the powders were dried, crushed, and sieved through a 200-mesh screen. The total proportion of sintering aids in the mixing powder was 4~8%.

In the ALD method, the ALD processes were performed in a custom-made rotary centrifugal reactor (ABScale-F001, self-developed, Wuhan, China), which was described in previous studies [16]. Trimethylaluminum (C_3H_9Al or TMA, purity of 99.9999%) and water (H_2O) were selected as the precursors to deposit Al_2O_3 on SiC (denoted as SiC@Al_2O_3), and the optimal deposition process was further investigated. In this method, only Al_2O_3 was used as the sintering aid, with a proportion of 4~8%.

In addition to the single mechanical mixing and ALD methods, some samples were first deposited with a portion of Al_2O_3 using ALD, followed by mechanical mixing with the remaining Al_2O_3 and Y_2O_3. The total ratio of Al_2O_3 to Y_2O_3 was also controlled at 1:1, and the total amount of sintering aids added remained at 4~8%.

The mixture of powders prepared using different methods was then loaded into the graphite molds for SPS (HPD25-SI, FCT Systeme GmbH, Frankenblick, Germany). The heating rate was 50~100 °C/min; the maximum sintering temperature was 1750~1950 °C; the sintering pressure was 20 MPa, and the sintering atmosphere was high-purity Ar (99.9999%). A holding stage was set at 1400 °C for 2~5 min. As illustrated in reference [10], the holding stage at around 1400 °C allowed Al_2O_3 and Y_2O_3 to react fully, forming a uniformly distributed YAG phase, which promoted the rapid densification of the samples. It should be clarified that the 1:1 mass ratio of Al_2O_3 to Y_2O_3 indicated that the atomic ratio of Al to Y was ~2.22:1. Compared to the atomic ratio of Al to Y in the YAG phase (5:3), Al was actually in relative excess. When YAG was at the desired phase, the 1:1 mass ratio was chosen to balance reactivity and liquid phase formation. The extended dwell time at 1400 °C ensured that excess Al_2O_3 compensated for stoichiometric deviations, facilitating YAG phase formation, as confirmed in [10].

2.3. Characterizations

The morphology of different powders was characterized using a scanning electron microscope (SEM, Nova NanoSEM 450, FEI, Lausanne, Switzerland) and a transmission electron microscopy (TEM, Tecnai G2 F30 electron microscope, FEI). The elemental distribution of the samples was observed via energy dispersive X-ray spectroscopy (EDS, Nova NanoSEM 450, FEI). The X-ray diffraction (XRD, XRD-6100, Shimadzu, Kyoto, Japan) patterns were used to analyze the crystal structure and phase composition of the samples with a Cu Kα1 radiation source and a scanning range of 20°~80°. The particle size distribution of the powder samples was measured using a laser diffraction particle analyzer (LDPA, Mastersizer 3000, Malvern Panalytical, Malvern, UK). The specific surface area was acquired through Brunner–Emmet–Tellet (BET) measurements (ASAP 2460, Micromeritics, Norcross, GA, USA).

The density of the samples was detected using the Ultrapycnometer 1000 density analyzer (Quantachrome, Boynton Beach, FL, USA) based on Archimedes's principle and Boyle's law. Thermal conductivity was determined by the product of the specific heat, the thermal diffusion coefficient, and the density of the sample. The specific heat and the thermal diffusion coefficient were measured using the comprehensive thermal analyzer (NETZSCH, Exton, PA, USA) and the LFA457 laser-pulsed thermal conductivity meter (NETZSCH), respectively.

The concentration of Al in the coating layer was determined by the inductive coupled plasma emission spectrometer (ICP-OES, PerkinElmer Avio 220 Max, Waltham, MA, USA), and the thickness of the Al_2O_3 coating was measured as follows: The total mass of the metallic element was calculated based on the concentration of Al and the total powder mass. Subsequently, the mass of the metal was converted into the mass of the corresponding oxide using the mass ratio of Al to O in Al_2O_3, and the volume of the oxide was derived from its theoretical density. Finally, assuming a uniform oxide coating on the powder surface, the average thickness of the coating was estimated by dividing the oxide volume by the total specific surface area of the powder.

3. Results

3.1. Features of the Raw SiC Powder

The specific surface area, particle size distribution, crystal structure, and SEM images of raw SiC powders were first systematically examined. For S-SiC, the specific surface area was 22.8 m^2/g, while L-SiC exhibited a specific surface area of 5.5 m^2/g, indicating that smaller particles possess higher surface areas and are prone to agglomeration. Laser diffraction analysis revealed a bimodal particle size distribution (Figure 1a), suggesting distinct particle size populations and agglomeration. The combination of large and small particles could improve packing efficiency by filling interstices and acquiring nanocrystals. This approach aligns with established practices in ceramic sintering to minimize porosity, as investigated in previous studies [10]. SEM images (Figure 1b,c) further confirmed agglomeration despite the uniform morphology of the raw particles.

XRD analysis (Figure 2) confirmed that both L-SiC and S-SiC particles retained the typical 3C-SiC phase without detectable phase transitions or impurity peaks, indicating minimal impact of particle size or agglomeration on the crystal structure.

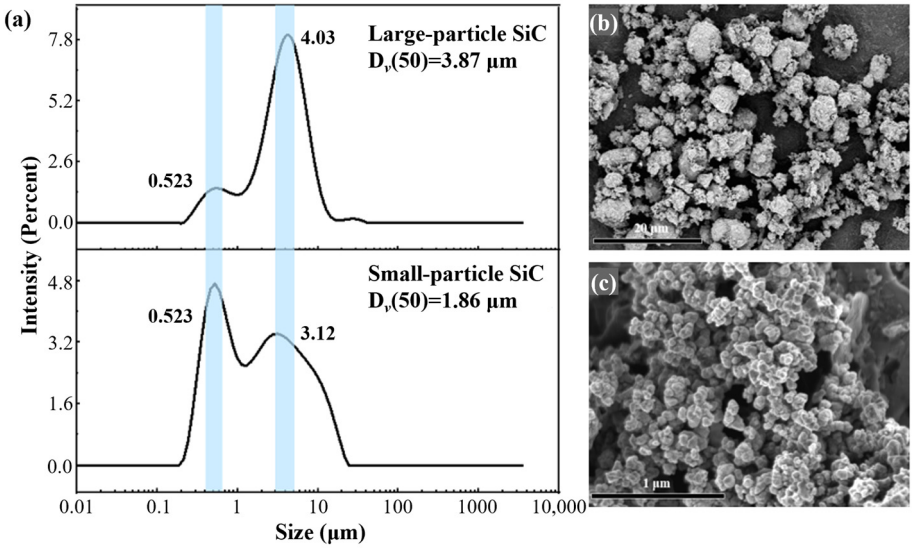

Figure 1. (**a**) Particle size distribution of L-SiC and S-SiC; (**b**) SEM of L-SiC; (**c**) SEM of S-SiC.

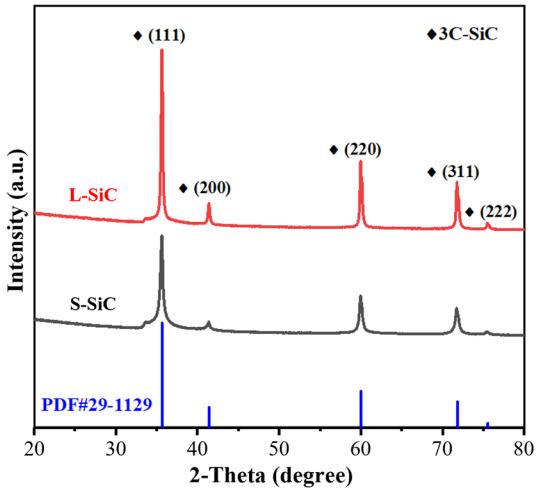

Figure 2. XRD patterns of the L-SiC and S-SiC powders.

3.2. Optimization of the Atomic Layer Deposition Process

Al_2O_3 films were deposited on SiC surfaces via ALD at 150 °C using TMA and H_2O as precursors. To address challenges in depositing films on high-surface-area powders, a "pressure-holding" step was incorporated (Figure 3b). The pressure-holding process involved closing the carrier gas and vacuum pump before introducing the precursor, thereby halting the flow of gas within the chamber. At this point, an appropriate amount of the precursor was introduced to ensure thorough contact with the reaction substrate. Subsequently, the intake pipeline and vacuum pump were opened to purge any unreacted precursor material. The duration of contact between the precursor and the reactant after the gas flow was closed was referred to as the "pressure-holding time".

Growth process optimization for the ALD coating of Al_2O_3 on the surface of SiC was conducted. As illustrated in Figure 4a, for S-SiC, during the adjustment of the pulse time, both the pressure-holding time and the purge time were allocated sufficiently. When the pulse time was less than 15 s, the precursor failed to achieve saturated adsorption, resulting in a slower growth rate of Al_2O_3. However, increasing the precursor pulse time did not significantly alter the film growth rate, indicating that TMA reached saturated adsorption at around 15 s under the experimental conditions of 150 °C. Similarly, for the L-SiC powder process, it was found that 5 s was the saturation pulse time. The optimal coating processes

for Al_2O_3 on S-SiC and L-SiC were determined as follows (with a base pressure of 148 Pa): 15 s (TMA), 240 s (pressure-holding, 218 Pa), 120 s (purge), 15 s (H_2O), 240 s (pressure-holding, 190 Pa), and 120 s (purge) for S-SiC and 5 s (TMA), 120 s (pressure-holding, 180 Pa), 90 s (purge), 5 s (H_2O), 120 s (pressure-holding, 168 Pa), and 90 s (purge) for L-SiC, as shown in Figure 4b,c, respectively. S-SiC's higher surface area necessitated longer precursor pulse times (15 s) to achieve saturation, whereas L-SiC's larger particle size allowed for shorter pulses (5 s). Under these conditions, the Al_2O_3 film was able to coat the SiC surface linearly, with a coating rate of 0.09 nm per cycle.

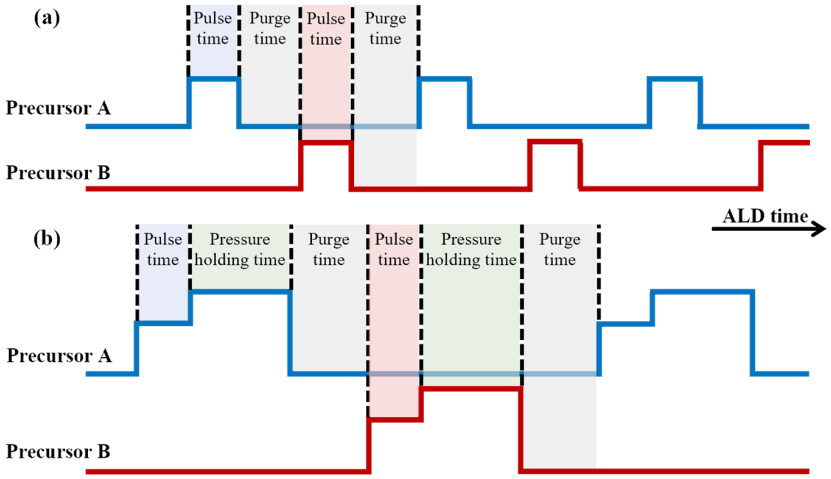

Figure 3. (**a**) Conventional ALD pulse process; (**b**) Pressure-holding ALD pulse process.

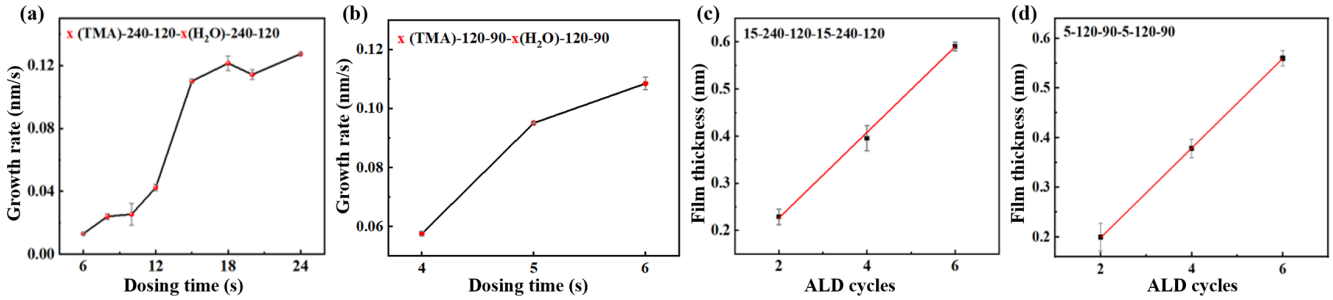

Figure 4. Growth rate vs. dosing time for (**a**) S-SiC and (**b**) L-SiC; Al_2O_3 film thickness vs. cycle number for (**c**) S-SiC and (**d**) L-SiC.

3.3. Morphological Characterization of SiC@Al_2O_3

The SEM and EDS images of S-SiC@Al_2O_3-15c (the cycle number was 15, and the theoretical deposition thickness was 1.35 nm) and L-SiC@Al_2O_3-30c (the cycle number was 30, and the theoretical deposition thickness was 2.70 nm) are shown in Figure 5. Post-coating, SiC surfaces exhibit a smooth morphology with enhanced brightness (Figure 5a,c). This is closely related to the high density of the Al_2O_3 layer and its unique optical scattering effect. The variation in brightness reflects the compactness of the Al_2O_3 layer structure, which contributes to enhancing the surface properties of the SiC powder. It is worth noting that the edges of the SiC particles become smoother after the coating process, with the originally sharp corners being effectively blunted. This indicates that the Al_2O_3 coating layer significantly improves the surface roughness of SiC. EDS results (Figure 5b,d) show that Al and O are uniformly distributed on the surface of the particles, and all particles are completely coated. This further demonstrates the high-quality deposition of the Al_2O_3 film.

Further in-depth structural characterization of the samples was conducted using TEM and TEM-EDS. The thickness of the Al_2O_3 coating layer was observed and manually

measured using TEM, and the results showed that it was consistent with the theoretical growth rate, thereby further confirming the precise control of the ALD process. At high resolution, a small portion of the bare SiC surface was observed to be oxidized, as shown in Figure 6c, forming an amorphous layer of silicon dioxide (SiO_2) of about 2.4 nm. This may be attributed to spontaneous oxidation resulting from the sample's exposure to an oxidizing environment due to improper storage. The elemental analysis using TEM-EDS further confirmed that the Al_2O_3 coating was highly uniform on the surface of individual SiC particles, with Al and O evenly distributed at the particle interface without any noticeable thickness variations or defects. This result is in good agreement with the earlier surface analysis using SEM, demonstrating the high efficiency and uniformity of the ALD coating process.

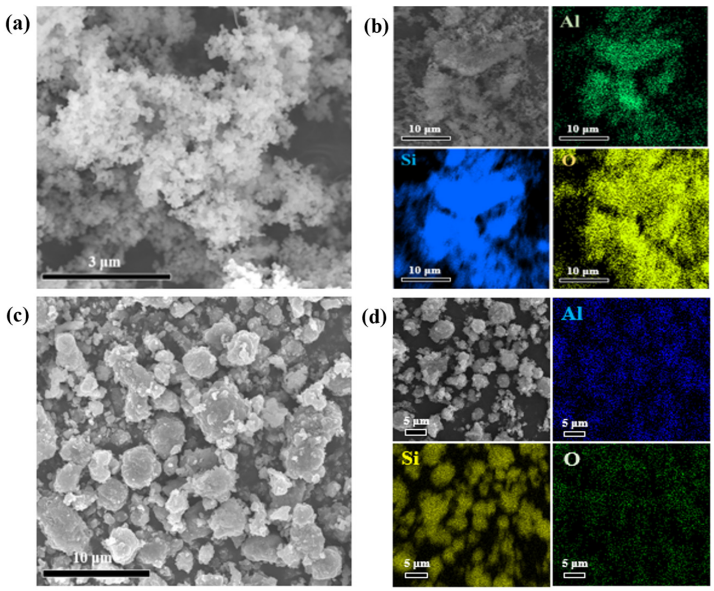

Figure 5. (**a**) SEM of S-SiC@Al_2O_3-15c; (**b**) EDS of S-SiC@Al_2O_3-15c; (**c**) SEM of L-SiC@Al_2O_3-30c; (**d**) EDS of L-SiC@Al_2O_3-30c.

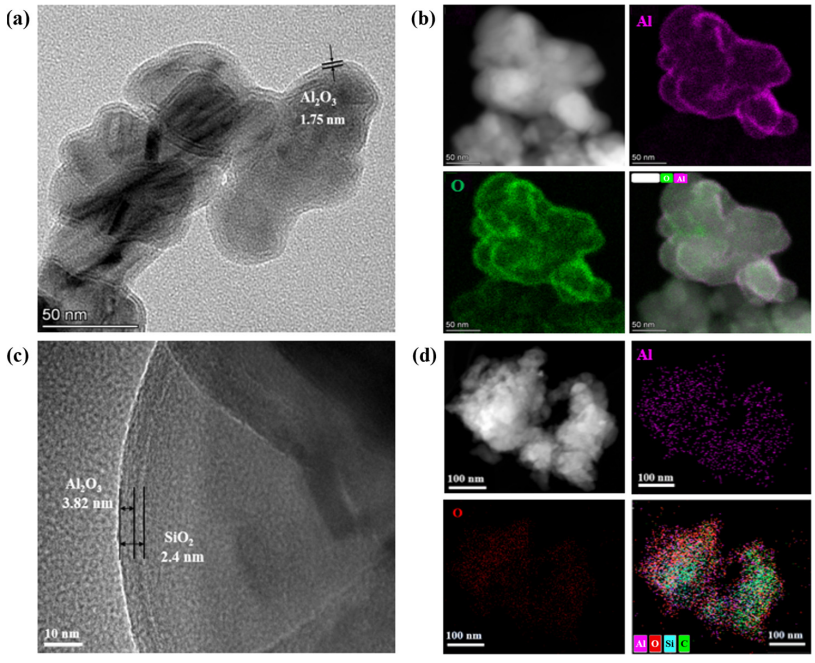

Figure 6. (**a**) TEM of S-SiC@Al_2O_3-15c; (**b**) TEM-EDS of S-SiC@Al_2O_3-15c; (**c**) TEM of L-SiC@Al_2O_3-30c; (**d**) TEM-EDS of L-SiC@Al_2O_3-30c.

3.4. Sintering and Performance Testing of SiC Pellets

As investigated in former studies [10], S-SiC and L-SiC particles were blended at a 1:1 mass ratio and mixed with Al_2O_3 and Y_2O_3 sintering aids to enhance sintering densification and thermal conductivity. The SEM-EDS and TEM images of mechanically mixed samples are shown in Figure 7. It was found that prior mechanical mixing led to inhomogeneous additive distribution and localized SiO_2 formation. The uneven SiO_2 layer might affect the sintering density and thermal conductivity of the sample. By contrast, ALD-coated SiC combined with Y_2O_3 mechanically mixing could achieve more uniform Al_2O_3 coverage, which was also possible to prevent the surface oxidation of SiC particles and enhance the sintered density by improving the interfacial bonding between particles. The ALD-Al_2O_3 layer might act as a diffusion barrier, isolating SiC surfaces from ambient oxygen and moisture. This prevented oxidative reactions during storage and sintering.

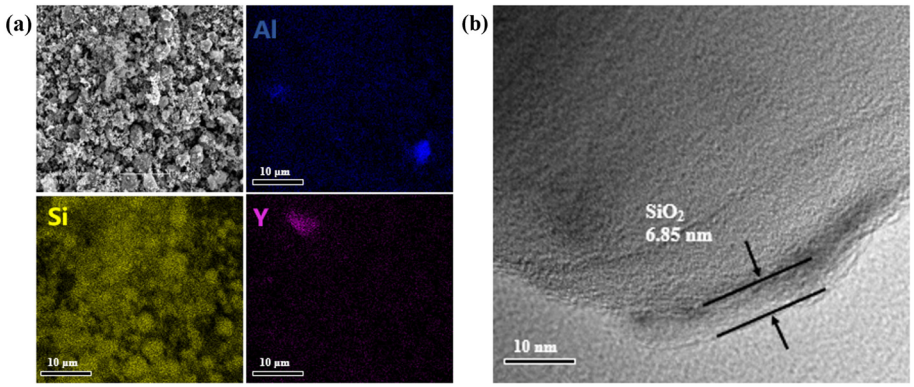

Figure 7. (**a**) SEM-EDS of mechanically mixed sample; (**b**) TEM of mechanically mixed sample.

To verify the potential beneficial effects of the ALD process on the sintering of the SiC matrix, the morphology and microstructure of the mixed powders were characterized in detail using SEM and TEM after the ALD process was employed to coat the Al_2O_3 and mechanically mixed it with Y_2O_3, as shown in Figure 8. The SEM images revealed that the Al_2O_3 deposited by ALD was uniformly distributed and smooth on the surface of the SiC particles, with Y_2O_3 enriched in some localized areas. TEM observations clearly demonstrated the integrity and uniformity of the Al_2O_3 layer and showed no significant oxide layer formation at the particle interfaces, thereby confirming the effectiveness of the ALD process in suppressing oxidation.

SiC powders mixed with sintering aids were prepared using mechanical mixing, ALD, and a combination of ALD and mechanical mixing, where the mass ratio of L-SiC and S-SiC was maintained at 1:1. The mixed powders were then densified using SPS under the same sintering procedures.

After sintering, the densities and thermal conductivities of different SiC matrix samples were measured, as shown in Table 1 and Figure 9, respectively. The reported density and thermal conductivity values represent the averages of triplicate measurements, with uncertainties of $\pm 1.5\%$ and $\pm 3\%$, respectively, based on instrument specifications and calibration protocols. The theoretical densities were calculated based on the mass ratios of SiC, Al_2O_3, and Y_2O_3 in the samples, as well as their respective theoretical densities. The relative densities were obtained by dividing the measured densities by the theoretical densities.

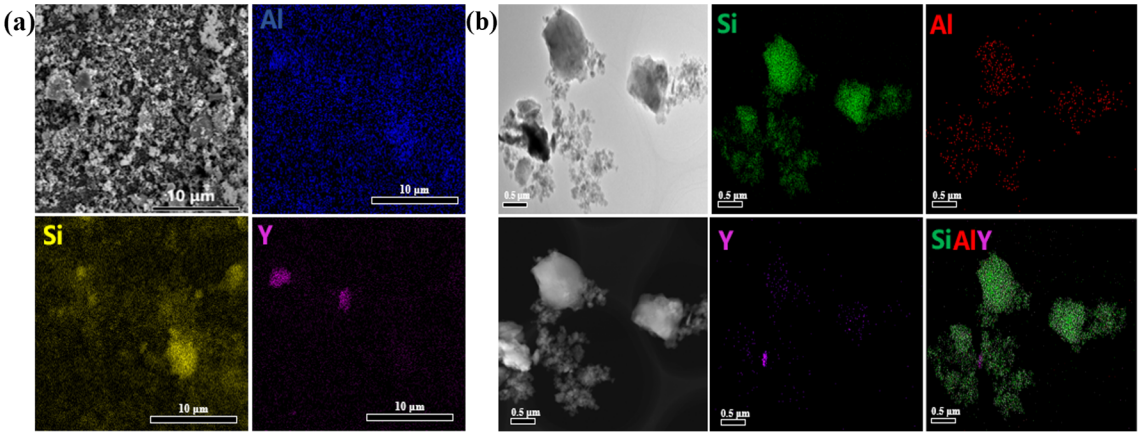

Figure 8. (**a**) SEM-EDS of ALD-coated and Y_2O_3-mixed powder sample; (**b**) TEM-EDS of ALD-coated and Y_2O_3-mixed powder sample.

Table 1. Relative densities of the sintered SiC matrix samples.

No.	Composition of Sintering Aids	Total Amount of Sintering Aids (wt.%)	Relative Density (% T.D.)	Porosity (%)
1	2.0% [1] Al_2O_3 + 2.0% Y_2O_3	4.0	80.61	13.71
2	3.0% Al_2O_3 + 3.0% Y_2O_3	6.0	90.09	6.89
3	4.0% Al_2O_3 + 4.0% Y_2O_3	8.0	95.79	1.10
4	2.0% ALD-Al_2O_3 [2] + 2.0 Y_2O_3	4.0	82.24	12.95
5	2.5% ALD-Al_2O_3 + 2.5 Y_2O_3	5.0	92.93	3.95
6	3.5% ALD-Al_2O_3 + 3.5 Y_2O_3	7.0	92.57	4.21
7	3.0% ALD-Al_2O_3 + 1.0% Al_2O_3 + 4.0% Y_2O_3	8.0	95.18	1.11
8	2.0% ALD-Al_2O_3 + 2.0% Al_2O_3 + 4.0% Y_2O_3	8.0	94.87	1.19

[1] The percentage of the powders indicates the mass percentage. [2] ALD-Al_2O_3 indicates Al_2O_3 deposited using the ALD method, and the others refer to Al_2O_3 (or Y_2O_3) mixed using the mechanical mixing method.

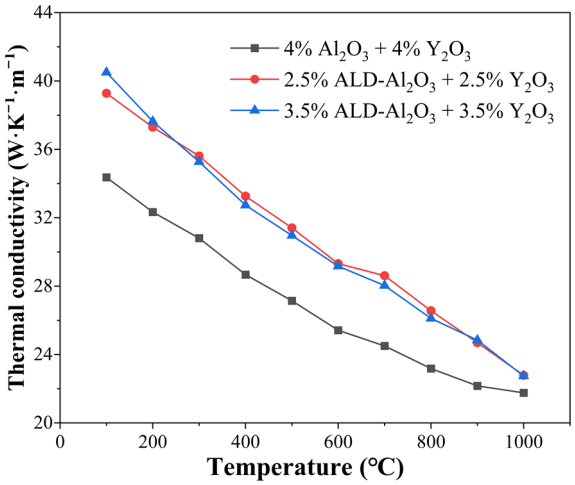

Figure 9. Corrected thermal conductivities of the sintered SiC matrix samples.

According to Table 1, the SiC matrix samples with the addition of 8 wt.% sintering aids have the highest density. Among them, the sample prepared using mechanically mixed powders (sample 3) has a slightly higher density than the samples prepared using powders mixed via ALD + mechanical mixing (samples 7 and 8). The densities of samples 2, 5, and 6 are slightly lower, but all exceed 90%. Among them, samples 5 and 6, which were prepared

with ALD-coated Al_2O_3 and mechanically mixed Y_2O_3, have higher densities. However, the total amount of sintering aids in these samples is not necessarily higher than that in sample 2. This suggests that ALD technology may be beneficial for improving the sintered density of the samples when the number of sintering aids is not very high. When the total amount of sintering aids is only 4%, as in samples 1 and 4, the density of the samples is very low regardless of whether mechanical mixing or ALD was used for blending. This indicates that a certain number of sintering aids are still necessary to improve the density of the samples. The density test results of different samples can preliminarily suggest that the ALD coating may have a certain positive effect on improving the sintered density of SiC matrix samples. However, the content of ALD-coated Al_2O_3 needs to be controlled within a certain range to achieve the desired effect.

Figure 9 shows the corrected thermal conductivity of samples 3, 5, and 6 listed in Table 1. The thermal conductivity was corrected for porosity using the Maxwell–Eucken theoretical model, with the formula as follows [15,24]:

$$\kappa_{\text{dense}} = \kappa_{\text{eff}}/[1 - 3\phi/(2 - \phi)], \quad (1)$$

where κ_{eff} is the measured thermal conductivity (including porosity), κ_{dense} is the corrected thermal conductivity of the dense material (porosity-free), and ϕ is the porosity (volume fraction).

It can be seen that although the densities of samples 5 and 6 are lower than that of sample 3 (still above 92%), their corrected thermal conductivity was improved to a certain extent compared to sample 3. At 100 °C, the thermal conductivity was increased by approximately 14~18%.

Based on the detection results of density and thermal conductivity, XRD and SEM tests were specifically conducted on samples 3 and 6, with the results shown in Figures 10 and 11. The main phase of the mechanically mixed samples and the ALD-7 wt.% Al_2O_3 samples after sintering did not change significantly compared to the unsintered SiC powder. The peaks at 35.6°, 41.4°, 60.0°, 71.8°, and 75.5° were, respectively, attributed to the (111), (200), (220), (311), and (222) crystal planes of SiC-3C (PDF#29-1129). During the sintering process, the liquid phase formed by the ALD-coated alumina was more uniform than that formed by mechanical mixing, which facilitated material transfer between SiC particles, allowing the SiC particles to grow more easily. Therefore, the XRD results showed that the ALD-7 wt.% Al_2O_3 sample had a higher main peak intensity of the SiC-3C phase compared to the mechanically mixed sample. The mechanically mixed sample exhibited an Al_2O_3 peak at 47.6° (PDF#46-1215), while the peaks at 44.7° and 49.3° were attributed to the SiC phase formed during the sintering process (PDF#50-1349). In the XRD pattern of the ALD-7 wt.% Al_2O_3 sample, the diffraction peaks at 60°, 71.8°, and 75.5° were split. This phenomenon was attributed to the wavelength difference between the Kα_1 and Kα_2 of the X-ray source. According to Bragg's equation ($2d\sin\theta = n\lambda$), as the diffraction angle (2θ) increases, the separation ($\Delta\theta$) of the diffraction angles for the same crystal plane for the two wavelengths significantly increases, causing the diffraction peak of a single crystal plane to split into two peaks that correspond to Kα_1 and Kα_2 in the high-angle region ($2\theta > 60°$).

By comparing the SEM microstructures in Figure 11a,b, it was found that the sample with ALD-deposited 7 wt.% Al_2O_3 exhibited clearer grain boundary contours and more significant grain growth compared to the sample with mechanically mixed 4 wt.% Al_2O_3 + 4 wt.% Y_2O_3, which is consistent with the aforementioned XRD results. The EDS elemental mapping results in Figure 11 further indicated that the distribution of Al elements in the ALD-prepared samples was more uniform.

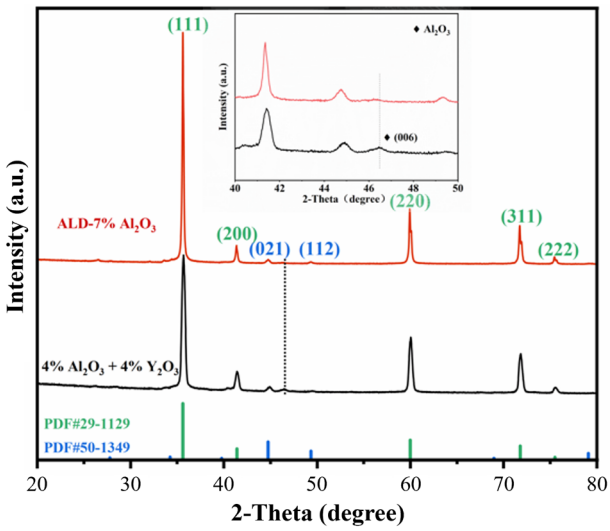

Figure 10. The XRD patterns of the sintered samples 3 and 6.

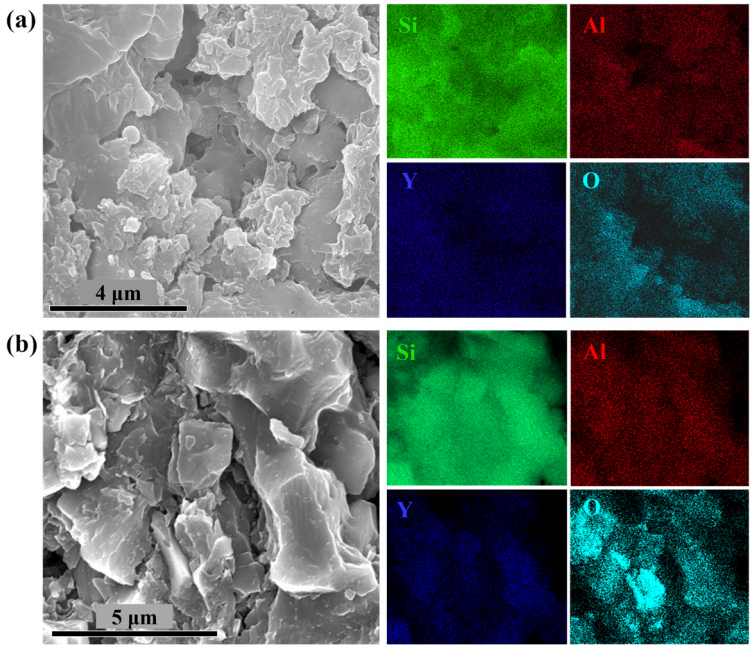

Figure 11. SEM-EDS figures of (**a**) sample 3 and (**b**) sample 6.

4. Discussion

This study demonstrates that ALD of Al_2O_3 coatings improves thermal conductivity by 14~18% (Figure 9), primarily due to reduced interfacial phonon scattering enabled by uniform Al_2O_3 distribution (Figures 5 and 6). The modest density improvement (~3%) aligns with prior studies on SiC-Y_2O_3-Al_2O_3 systems, where interfacial homogeneity—not bulk densification—drives thermal gains. By optimizing pressure-holding ALD protocols, the precise control of Al_2O_3 coating thickness (0.09 nm/cycle) and uniformity were achieved, as validated by TEM and SEM analyses (Figures 5 and 6). The ALD coating reduces the surface roughness and agglomeration of SiC particles (Figure 5a,c), enabling tighter particle arrangements. Smoother surfaces could minimize interparticle friction and improve interfacial contact during sintering.

Due to the differences in porosity among samples prepared using different processes (e.g., mechanically mixed samples exhibit higher porosity), we have corrected the thermal conductivity data using the Maxwell–Eucken model to eliminate the influence of porosity.

The corrected results show that the dense material thermal conductivity of ALD-coated samples (e.g., sample 5, 6) is still approximately 14~18% higher than that of mechanically mixed samples (sample 3). Below, the key mechanisms driving these improvements are discussed.

1. Suppression of interfacial oxidation

The ALD-Al_2O_3 coatings suppressed the formation of detrimental SiO_2 layers on SiC surfaces. TEM-EDS analysis revealed that ALD-coated samples exhibited SiO_2 layers that were ~2 nm thick (Figure 6c), whereas mechanically mixed samples showed discontinuous SiO_2 layers (~5 nm, Figure 7b). These thicker SiO_2 layers might act as thermal barriers due to their low intrinsic thermal conductivity (~1.4 W/m·K), aligning with prior studies on SiC-based ceramics [10,15]. By minimizing interfacial oxidation, ALD preserves the high thermal conductivity of SiC, which is critical for nuclear fuel applications.

2. Enhanced additive distribution and YAG phase formation

The uniform distribution of Al_2O_3 via ALD (Figures 5 and 8) facilitated the formation of a homogeneous YAG ($Y_3Al_5O_{12}$) phase during sintering. This is attributed to the additional Al_2O_3 deposited by ALD. ALD-deposited Al_2O_3 adjusted the Al/Y atomic ratio closer to YAG's stoichiometry (5:3), enhancing phase homogeneity. The YAG phase, with its lower melting point (1760 °C), promoted efficient liquid-phase sintering, as evidenced by the higher relative densities of ALD-coated samples (Table 1, Samples 5~6). In contrast, mechanically mixed samples exhibited localized Y_2O_3 agglomeration (Figure 7a), leading to inhomogeneous YAG formation and suboptimal densification.

3. Thermal conductivity enhancement via interfacial engineering

The about 14~18% improvement in corrected thermal conductivity for ALD-coated samples (Figure 9) stems from two experimentally validated mechanisms:

Reduced phonon scattering: uniform Al_2O_3 coatings minimized lattice mismatches and SiO_2 clusters at SiC interfaces, lowering phonon scattering (Figure 5).

Optimized heat flow pathways: Excess Al_2O_3 from ALD shifted the Al/Y ratio toward YAG's stoichiometry (5:3), promoting homogeneous liquid-phase sintering. Mechanically mixed samples exhibited localized Y_2O_3 agglomeration (Figure 7a), leading to incomplete YAG formation and suboptimal densification.

While ALD-coated Al_2O_3 improved thermal conductivity, excessive or insufficient coating thickness compromised the sintered density (Table 1). At 5~7 wt.% ALD-Al_2O_3 + Y_2O_3, the balance between YAG phase formation and intergranular phase content was optimal. Higher Al_2O_3 concentrations introduced low-thermal-conductivity intergranular phases, while lower amounts insufficiently promoted liquid-phase sintering. This highlights the importance of precise ALD control to optimize both density and thermal performance.

This study also points out the possible directions for future research:

- Interfacial characterization: employ advanced techniques such as atomic-resolution TEM or X-ray photoelectron spectroscopy to elucidate bonding mechanisms at the Al_2O_3/SiC interface.
- Al_2O_3-Y_2O_3 co-deposition via ALD: Explore the ALD process for the sequential or composite coating of Al_2O_3 and Y_2O_3 on SiC powders. Based on the research results presented in this work, this approach is expected to enhance the uniformity of the YAG phase during sintering while mitigating the influence of Al_2O_3 on the thermal conductivity of the SiC matrix.
- Scalability studies: transition from lab-scale ALD to pilot-scale systems to evaluate industrial feasibility and cost-performance trade-offs.

- Long-term stability testing: expose ALD-coated SiC pellets to simulated reactor conditions (high temperature, irradiation, mechanical stress, etc.) to assess durability over extended periods.
- Environmental impact mitigation: develop eco-friendly ALD precursors and recycling protocols to minimize chemical waste and align with sustainable manufacturing practices.

Addressing these directions will bridge the gap between laboratory achievements and practical implementation, ultimately advancing the development of high-performance SiC-based materials for next-generation accident-tolerant fuels.

5. Conclusions

This work demonstrates that ALD of Al_2O_3 coatings enhances the thermal conductivity of SiC matrix pellets by 14~18% at 100 °C, with sintered densities exceeding 92% T.D. These findings underscore ALD's potential for advancing SiC-based accident-tolerant fuels. By optimizing ALD protocols, uniform Al_2O_3 layers were achieved, mitigating detrimental SiO_2 formation and improving interfacial bonding during SPS. Key findings include the following:

- The use of pressure-holding ALD protocols could effectively deposit Al_2O_3 on SiC, with a good deposition effect and a deposition rate of approximately 0.09 nm/cycle.
- ALD-Al_2O_3 + Y_2O_3 (5~7 wt.%) increased thermal conductivity by 14~18% compared to traditional mechanical mixing, despite slightly lower densities, highlighting the critical role of interfacial uniformity in reducing phonon scattering.
- A balance between sintering aid concentration and ALD-driven uniformity is essential, as excessive or insufficient Al_2O_3 content adversely affects densification.

Future studies should focus on interfacial bonding mechanisms, the co-deposition of Al_2O_3-Y_2O_3 via ALD, and scalability to industrial processes. Additionally, long-term stability under reactor conditions and environmental impact mitigation strategies warrant further exploration. This research advances the development of high-performance SiC-based fuels, contributing to safer and more efficient next-generation nuclear reactors.

Author Contributions: Conceptualization, Y.Z. and X.L.; methodology, Y.Z. and X.L.; validation, J.W., W.W. and Y.Z.; formal analysis, J.W., W.W., Y.L. and Z.L.; investigation, W.W., J.W., Y.Z., Y.L. and Z.L.; resources, R.C. and W.L.; data curation, Y.Z. and X.L.; writing—original draft preparation, Y.Z. and W.W.; writing—review and editing, J.W., X.L., R.C. and W.L.; visualization, W.W., Y.Z., Y.L. and Z.L.; supervision, W.L. and R.C.; project administration, Y.L. and Z.L.; funding acquisition, W.L.; conceptualization, R.C. All authors have read and agreed to the published version of the manuscript.

Funding: This research received no external funding.

Data Availability Statement: The original contributions presented in this study are included in the article. Further inquiries can be directed to the corresponding authors.

Acknowledgments: The authors are grateful to China North Nuclear Fuel Co., Ltd. for its independent financial support of this study, which has provided an important safeguard for the implementation of the project. We would also like to thank Zongyi Shao and Shuaishuai Feng for their efforts in the early stages of the project.

Conflicts of Interest: Author Yumeng Zhao, Jiquan Wang, Yu Li, Zongshu Li and Wei Liu were employed by the company China North Nuclear Fuel Co., Ltd. The remaining authors declare that the research was conducted in the absence of any commercial or financial relationships that could be construed as a potential conflict of interest.

References

1. Terrani, K.A. Accident Tolerant Fuel Cladding Development: Promise, Status, and Challenges. *J. Nucl. Mater.* **2018**, *501*, 13–30. [CrossRef]
2. Ko, J.; Kim, J.W.; Min, H.W.; Kim, Y.; Yoon, Y.S. Review of Manufacturing Technologies for Coated Accident Tolerant Fuel Cladding. *J. Nucl. Mater.* **2022**, *561*, 153562. [CrossRef]
3. Zhang, X.; Pan, X.; Lu, Y.; Zhang, R. Preparation and research progress of accident tolerant fuel pellets. *Powder Metall. Technol.* **2022**, *40*, 334–339, 350. [CrossRef]
4. Snead, L.L.; Venneri, F.; Kim, Y.; Terrani, K.A.; Tulenko, J.E.; Forsberg, C.W.; Peterson, P.F.; Lahoda, E.J. Fully Ceramic Microencapsulated Fuels: A Transformational Technology for Present and next Generation Reactors. *Trans. Am. Nucl. Soc.* **2011**, *104*, 4.
5. Terrani, K.A.; Snead, L.L.; Gehin, J.C. Microencapsulated Fuel Technology for Commercial Light Water and Advanced Reactor Application. *J. Nucl. Mater.* **2012**, *427*, 209–224. [CrossRef]
6. Terrani, K.A.; Kiggans, J.O.; Silva, C.M.; Shih, C.; Katoh, Y.; Snead, L.L. Progress on Matrix SiC Processing and Properties for Fully Ceramic Microencapsulated Fuel Form. *J. Nucl. Mater.* **2015**, *457*, 9–17. [CrossRef]
7. Lee, Y.; Cho, B.; Cho, N.Z. Steady- and Transient-State Analyses of Fully Ceramic Microencapsulated Fuel with Randomly Dispersed Tristructural Isotropic Particles via Two-Temperature Homogenized Modeld I: Theory and Method. *Nucl. Eng. Technol.* **2016**, *48*, 650–659. [CrossRef]
8. Olander, D. Nuclear Fuels-Present and Future. *J. Nucl. Mater.* **2009**, *389*, 1–22. [CrossRef]
9. Cao, F.; Fan, X.; Liu, B.; Zhao, X.; Guo, F.; Xiao, P. Microstructure and Thermal Conductivity of Fully Ceramic Microencapsulated Fuel Fabricated by Spark Plasma Sintering. *J. Am. Ceram. Soc.* **2018**, *101*, 4224–4236. [CrossRef]
10. Liu, W.; Shao, Z.; Liu, W.; Meng, Y.; Feng, S.; Cai, Z. Study on performance of coated particle dispersed fuel pellet prepared by spark plasma sintering. *At. Energy Sci. Technol.* **2023**, *57*, 1810–1816.
11. Terrani, K.A.; Kiggans, J.O.; Katoh, Y.; Shimoda, K.; Montgomery, F.C.; Armstrong, B.L.; Parish, C.M.; Hinoki, T.; Hunn, J.D.; Snead, L.L. Fabrication and Characterization of Fully Ceramic Microencapsulated Fuels. *J. Nucl. Mater.* **2012**, *426*, 268–276. [CrossRef]
12. Lee, J.K.; Kang, H.H.; Shim, D.J.; Lee, E.G.; Kim, H. Effects of YAG-Phase Amount on the Microstructure and Phase Transformation during the Liquid-Phase Sintering of β-SiC. *Key Eng. Mater.* **1999**, *161–163*, 263–266. [CrossRef]
13. Gao, L.; Wang, H.; Kawaoka, H.; Sekino, T.; Niihara, K. Fabrication of YAG-SiC Nanocomposites by Spark Plasma Sintering. *J. Eur. Ceram. Soc.* **2002**, *22*, 785–789. [CrossRef]
14. Zhang, N.; Liu, H.; Xiaoyang, W.; Kan, H.; Long, H. Sintering Density of SiC-YAG Ceramic Composite Material. *Bull. Chin. Ceram. Soc.* **2015**, *34*, 2125–2129, 2138.
15. Chai, Z.; Gao, Z.; Liu, H.; Zhang, X.; Glodan, G.; Xiao, P. Thermal Conductivity of Spark Plasma Sintered SiC Ceramics with Alumina and Yttria. *J. Eur. Ceram. Soc.* **2021**, *41*, 3264–3273. [CrossRef]
16. Duan, C.-L.; Liu, X.; Shan, B.; Chen, R. Fluidized Bed Coupled Rotary Reactor for Nanoparticles Coating via Atomic Layer Deposition. *Rev. Sci. Instrum.* **2015**, *86*, 075101. [CrossRef]
17. George, S.M. Atomic Layer Deposition: An Overview. *Chem. Rev.* **2010**, *110*, 111–131. [CrossRef]
18. Zhang, J.; Li, Y.; Cao, K.; Chen, R. Advances in Atomic Layer Deposition. *Nanomanuf. Metrol.* **2022**, *5*, 191–208. [CrossRef]
19. Cui, H.; Gong, L.; Sun, Y.; Yang, G.Z.; Liang, C.L.; Chen, J.; Wang, C.X. Direct Synthesis of Novel SiC@Al_2O_3 Core-Shell Epitaxial Nanowires and Field Emission Characteristics. *CrystEngComm* **2011**, *13*, 1416–1421. [CrossRef]
20. Shishkin, R.A. Oxide-Bonded Silicon Carbide and Alumina Ceramics Obtained from Template SCS Powders. *Ceram. Int.* **2025**, *51*, 10340–10350. [CrossRef]
21. Liu, Y.; Chen, Z.; Liu, R.; Zhao, J.; Liu, M. Preparation of SiC@Al_2O_3–Y_2O_3 Core-Shell Nanoparticles by a Slow Precipitation Method for Dense SiC Sintering. *Ceram. Int.* **2020**, *46*, 24504–24511. [CrossRef]
22. Chen, H.; Fraser Stoddart, J. From Molecular to Supramolecular Electronics. *Nat. Rev. Mater.* **2021**, *6*, 804–828. [CrossRef]
23. Podder, S.; Basumatary, B.; Gogoi, D.; Bora, J.; Pal, A.R. Pyro-Phototronic Application in the Au/ZnO Interface for the Fabrication of a Highly Responsive Ultrafast UV Photodetector. *Appl. Surf. Sci.* **2021**, *537*, 147893. [CrossRef]
24. Progelhof, R.C.; Throne, J.L.; Ruetsch, R.R. Methods for Predicting the Thermal Conductivity of Composite Systems: A Review. *Polym. Eng. Sci.* **1976**, *16*, 615–625. [CrossRef]

Disclaimer/Publisher's Note: The statements, opinions and data contained in all publications are solely those of the individual author(s) and contributor(s) and not of MDPI and/or the editor(s). MDPI and/or the editor(s) disclaim responsibility for any injury to people or property resulting from any ideas, methods, instructions or products referred to in the content.